



Article

Ultrafast Dynamics of Demagnetization in FeMn/MnGa Bilayer Nanofilm Structures via Phonon Transport

Tianran Jiang ¹, Xupeng Zhao ², Zhifeng Chen ³, Yongyong You ¹, Tianshu Lai ^{1,*} and Jianhua Zhao ^{2,*}

¹ State Key Laboratory of Optoelectronic Materials and Technologies, School of Physics, Sun Yat-Sen University, Guangzhou 510275, China

² State Key Laboratory of Superlattices and Microstructures, Institute of Semiconductors, Chinese Academy of Sciences, P.O. Box 912, Beijing 100083, China

³ School of Physics and Electronic Engineering, Guangzhou University, Guangzhou 510006, China

* Correspondence: stslts@mail.sysu.edu.cn (T.L.); jhzhao@red.semi.ac.cn (J.Z.)

Abstract: Superdiffusive spin transport has been proposed as a new mechanism of ultrafast demagnetization in layered magnetic nanostructures and demonstrated experimentally. However, it is unknown if it is possible for phonon transport to occur and manipulate ultrafast demagnetization. Here, we explore the ultrafast dynamics of demagnetization of an antiferromagnet/ferromagnet bilayer nanostructure, of a FeMn/MnGa bilayer film prepared by molecular beam epitaxy. Ultrafast dynamics of a two-step demagnetization were observed through the time-resolved magneto-optical Kerr effect. The first-step fast component of the two-step demagnetization occurred within ~200 fs, while the second-step slow component emerged in a few tens of picoseconds. For a single MnGa film, only the ultrafast dynamics of the first-step fast demagnetization were observed, revealing that the second-step slow demagnetization originates from interlayer phonon transport. A four-temperature model considering phonon transport was developed and used to effectively reproduce the observed ultrafast dynamics of two-step demagnetization. Our results reveal the effect of phonon transport on demagnetization for the first time and open up a new route to manipulate ultrafast demagnetization in layered magnetic structures.



Citation: Jiang, T.; Zhao, X.; Chen, Z.; You, Y.; Lai, T.; Zhao, J. Ultrafast Dynamics of Demagnetization in FeMn/MnGa Bilayer Nanofilm Structures via Phonon Transport. *Nanomaterials* **2022**, *12*, 4088. <https://doi.org/10.3390/nano12224088>

Academic Editor: Yurii K. Gun'ko

Received: 16 October 2022

Accepted: 18 November 2022

Published: 20 November 2022

Publisher's Note: MDPI stays neutral with regard to jurisdictional claims in published maps and institutional affiliations.



Copyright: © 2022 by the authors. Licensee MDPI, Basel, Switzerland. This article is an open access article distributed under the terms and conditions of the Creative Commons Attribution (CC BY) license (<https://creativecommons.org/licenses/by/4.0/>).

Keywords: antiferromagnet/ferromagnet; nanofilm structures; phonon transport; ultrafast demagnetization; time-resolved magneto-optical Kerr effect

1. Introduction

Since a laser-induced ultrafast demagnetization was first demonstrated in a pioneering experiment on single Ni film [1], many studies have been carried out on different magnetic materials through a time-resolved magneto-optical Kerr effect (TR-MOKE), including FePt [2], CoPt [3], CrO₂ [4], GdFeCo [5], Co₂FeAl [6] and TbFeCo [7,8]. The laser-induced demagnetization is usually described by a three-temperature model (3T-M) in which the temperatures of electron, spin and lattice subsystems coupled to each other and their time evolution was described by a set of derivative equations, while the time evolution of the temperature of the spin subsystem described the ultrafast dynamics of magnetization after photon excitation [1,9,10]. However, the microscopic mechanisms of ultrafast demagnetization on femtosecond timescales are still being strongly debated. Several different mechanisms were presented, such as a direct coupling between light field and spin bath [11], coulomb-exchange spin flips [12] and phonon-mediated spin-flip processes [13], etc.

In recent years, a new superdiffusive spin transport mechanism was proposed to explain the ultrafast demagnetization process in layered magnetic structures [14], and has already been demonstrated successfully in ferromagnetic/nonmagnetic (FM/NM) [15–18] and ferromagnetic/ferromagnetic (FM/FM) [19,20] layered structures. Based on 3T-M, each FM layer contained three subsystems of electrons, spins and lattices, whereas an NM layer had only electron and lattice subsystems. Consequently, there might be other transports

occurring between different layers in layered magnetic structures besides a superdiffusive spin transport, such as hot electron transports and phonon transports. In fact, ultrafast demagnetization driven by a hot electron transport from an NM layer into an FM layer has already been observed in an NM/FM layered magnetic structure [21,22], where the NM layer was an Au [21] or Cu film [22], while the FM layer was a Ni [21] or [Co/Pt]_n [22] film. However, the ultrafast dynamics of demagnetization driven by phonon transports have not been observed and reported to our knowledge. Phonon transports may also open up a new route to manipulate ultrafast demagnetization in a layered magnetic structure, and thus are critical to explore. To observe the effect of phonon transports on ultrafast demagnetization, it is essential to suppress the effect of hot electron and spin transports. Therefore, the design of layered magnetic structure samples becomes very important and is the key factor which affects whether the phonon transport is observable or not.

In this paper, we designed an antiferromagnetic/ferromagnetic (AFM/FM) bilayer nanostructure, using FeMn/MnGa grown on a GaAs substrate and studied its ultrafast dynamics of demagnetization to attempt the observation of possible phonon transports. Here, the AFM layer of FeMn was chosen because Mn-based AFM materials, such as FeMn, PdMn, IrMn and PtMn, have an extremely short electron and spin diffusion length on the order of 1 nm [23–25] and have zero net magnetizations; thus, hot electron and spin transports are significantly suppressed. On the other hand, it was reported that the exchange bias field between the FeMn and MnGa layers disappeared at room temperature [26], thus avoiding a possible laser-induced magnetization change in the MnGa layer driven by the exchange bias field. Consequently, the ultrafast dynamics of demagnetization in an MnGa single layer could be observed after photoexcitations. We studied the ultrafast dynamics of demagnetization of FeMn/MnGa bilayer and MnGa single layer films comparatively using TR-MOKE. We indeed observed the ultrafast dynamics of two-step demagnetization in an FeMn/MnGa layered structure, while only the ultrafast dynamics of one-step demagnetization were observed in a single layer MnGa film. The second-step slower ultrafast demagnetization appeared only in FeMn/MnGa bilayer structure and had a time constant of ~10 ps, and was thus ascribed to the phonon transport from the FeMn layer because electron and spin transports were suppressed in this sample structure and usually took place within a subpicosecond time scale. We developed a four-temperature model by introducing the temperature of the phonon subsystem of an FeMn layer into the 3T-M and taking account for its coupling to the temperatures of electron, spin and phonon subsystems of the MnGa layers. Simulation calculations were performed based on the four-temperature model. The simulated results closely reproduced our experimental results of the ultrafast dynamics of two-step demagnetization, further confirming the origin of phonon transports of the second-step slower demagnetization. Therefore, we observed for the first time the effect of phonon transports on ultrafast demagnetization in a bilayer magnetic nanostructure.

2. Materials and Experimental Method

FeMn/MnGa bilayer films were deposited on GaAs film substrates by molecular-beam epitaxy (MBE), as described in detail in reference [26]. It was expected that an MBE-prepared sample could lead to a good interlayer phonon transport because a lattice match was required in MBE, so that almost no phonon scattering would occur at the magnetic interface of the FeMn/MnGa heterostructure. The sample structure consisted of FeMn (3 nm)/MnGa (8 nm)/GaAs (200 nm). Magnetic moments of MnGa film were dominated by only 3d electrons near the Fermi level [27], whereas FeMn was antiferromagnetic and had no net moments because the paired Fe and Mn atoms were arranged anti-parallel in the FeMn films, respectively [23,24].

The ultrafast dynamics of demagnetization were studied through TR-MOKE measurement. A laser pulse with a central wavelength of 800 nm, a duration of ~100 fs and a repetition rate of 1 kHz was generated from a Ti: sapphire regenerative amplifier. The laser pulse was divided into strong pump and weak probe with a pump/probe intensity

ratio larger than 20. The pump and probe pulses were incident on the sample almost normally, and focused on a spot of 150 μm and 75 μm for the pump and the probe, respectively. The polar Kerr rotation of the reflected probe light was detected by an optical balanced bridge and was measured by a lock-in amplifier synchronized to an optical chopper that modulated pump pulses at ~ 340 Hz. All measurements were performed at room temperature.

3. Results and Discussion

The magnetic properties of the sample were first characterized by polar MOKE and a vibrating sample magnetometer (VSM) with an external field applied perpendicularly to the surface of the sample. As shown in Figure 1, the normalized out-of-plane hysteresis loops present nearly square and centric-symmetric, and show a coercivity of ~ 4500 Oe, which reveal that this sample has a strong perpendicular magnetic anisotropy and a zero exchange bias field between the FeMn and MnGa layers at room temperature, consistent with a previous report [26]. The square out-of-plane hysteresis loops agree well with the sole MnGa film reported previously [27], revealing the completely antiferromagnetic property of FeMn. Therefore, the magnetic signal measured by MOKE and VSM originates from the sole MnGa layer, excluding the FeMn layer. In this way, we can study the time evolution of magnetization in the sole MnGa layer after the photoexcitation of FeMn/MnGa bilayered structures.

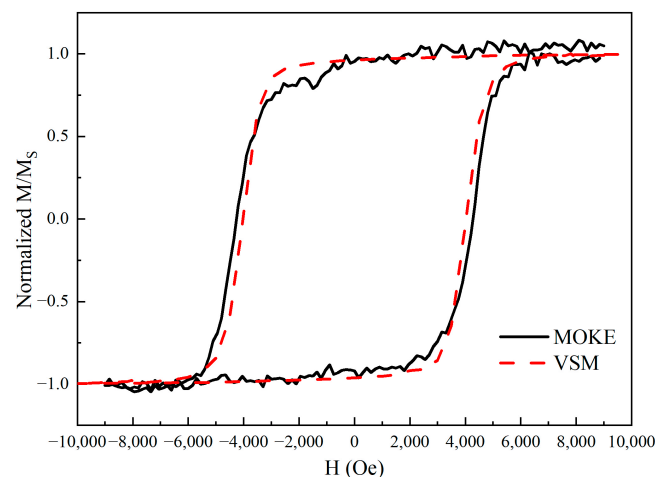


Figure 1. Measurement of the normalized out-of-plane hysteresis loops. The dash and solid loops are measured by VSM and MOKE, respectively.

The ultrafast dynamics of laser-induced demagnetization of the FeMn/MnGa layered structure was measured experimentally using TR-MOKE spectroscopy for different pump fluence levels under a saturation magnetic field of ~ 8000 Oe applied along the normal of the sample plane, and plotted in Figure 2. One can see that the ultrafast dynamics present a two-step ultrafast demagnetization process, including a fast demagnetization process occurring within a picosecond and a slower process in several tens of picoseconds, as the dot-dashed line shows. The amplitude of the two demagnetization processes increases with pump fluence. The fast demagnetization process is easily understood based on 3T-M [1] and can be ascribed to electron–spin coupling in the MnGa film layer. A similar fast demagnetization process was observed in many FM films, such as Ni [1], FePt [2] and CoPt [3]. However, the slower demagnetization process was not observed usually [1–3]. Here, there are two possible origins for the slower demagnetization process. One is an intralayer phonon–spin coupling interaction that re-heats spins in the MnGa layer based on 3T-M. Similar phenomena were observed in CrO_2 [4], Fe_3O_4 [28] and $\text{Mn}_2\text{Ru}_x\text{Ga}$ [29]. The other is interlayer transport. Electron and spin transports can be ruled out because they occurred in a subpicosecond time scale [15,17,19,20,22,30], whereas here the second-step slower demagnetization emerges over 10 ps. On the other hand, the FeMn layer

is antiferromagnetic, and has an extremely short electron and spin diffusion length of ~ 1 nm [23–25], suppressing electron and spin transports into the MnGa layer from the FeMn layer. As a result, only phonon transport becomes possible. Similar interlayer phonon transports were reported in a nonmagnetic bilayer structure of Pt/Au and indeed occurred in several tens of picoseconds [31].

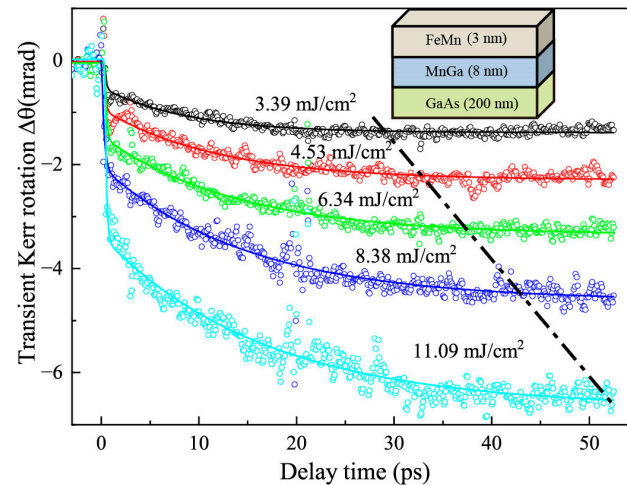


Figure 2. The pump–fluence dependence of TR-MOKE measurement in an FeMn/MnGa layered structure. The scattered open circles are Kerr signal measurements. The solid lines are the fittings to experimental profiles with a double exponential sum function described in the text (Equation (1)). The dot-dashed line joins the maximum demagnetization points at different pump fluence levels.

To distinguish intralayer phonon–spin coupling interaction from interlayer phonon transport, a comparative experiment was carried out on the layered FeMn/MnGa sample and a single layer MnGa (12 nm) film. The measured ultrafast dynamics are plotted in Figure 3a for the pump fluence of 8.38 mJ/cm^2 . It is very exciting that two entirely different ultrafast dynamics of magnetization emerged. The ultrafast dynamics of laser-induced magnetization of a single layer MnGa film presented one-step ultrafast demagnetization in a subpicosecond time scale followed by a slower recovery of magnetization, whereas the bilayer FeMn/MnGa film presented two-step demagnetization: one fast demagnetization process in a subpicosecond time scale and one slower demagnetization process in several tens of picoseconds. The disappearance of the second slower process in the sole MnGa film reveals a weak or negligible intralayer phonon–spin coupling interaction. Consequently, the second-step slower demagnetization process may only originate from phonon-mediated interlayer coupling or phonon transport because electron and spin transports are ruled out due to their appearance in a time scale of less than one picosecond [15,17,19,20,22,30] and the extremely short diffusion length of electrons and spins in the FeMn layer [23–25].

To directly determine that the first-step fast demagnetization process is relevant to electrons, and to validate that the second-step slower demagnetization process is not directly relevant to electrons, we measured the transient reflectivity and Kerr signal of FeMn/MnGa bilayer film, as the solid line and open circles shown in Figure 3b, respectively. Transient reflectivity mainly reflects the relaxation dynamics of the temperature of excited electrons. It presented one-step ultrafast decay within 0.8 ps followed by a slower recovery or the temperature of excited electrons rose fast within 0.8 ps and then decayed slowly. Meanwhile, the first-step fast demagnetization also finished within 0.8 ps and agreed well with ultrafast demagnetization in the sole MnGa layer, as shown in Figure 3a. Consequently, we can assert that the first-step fast demagnetization in the FeMn/MnGa bilayer nanostructure comes from ultrafast electron–spin coupling in the sole MnGa layer. However, transient reflectivity does not contain a slower second-step decay process. As a result, the second-step slower demagnetization process is not directly relevant to the excited electrons. Therefore, we can definitively conclude that the second-step slower demagnetization originates from the

phonon transport from FeMn into MnGa layers. Now, a clear physical picture can be drawn out. Photoexcited electrons transfer energy first into phonons in the FeMn and MnGa layers via electron–phonon coupling, and spins in MnGa layer via electron–spin coupling. The electron–spin coupling in the MnGa layer leads to the first-step subpicosecond ultrafast demagnetization. Then, phonon coupling between the FeMn and MnGa layers or phonon transport from the FeMn to the MnGa layers transfers further energy into the MnGa layer, which results in the emergence of the second-step slower demagnetization. However, we still do not know how phonon-mediated energy transfer from FeMn to MnGa layers reaches the spin subsystem in the MnGa layer, directly by phonon (FeMn)–spin (MnGa) coupling or indirectly by phonon (FeMn)–phonon (MnGa)–spin coupling? This will be further explored later.

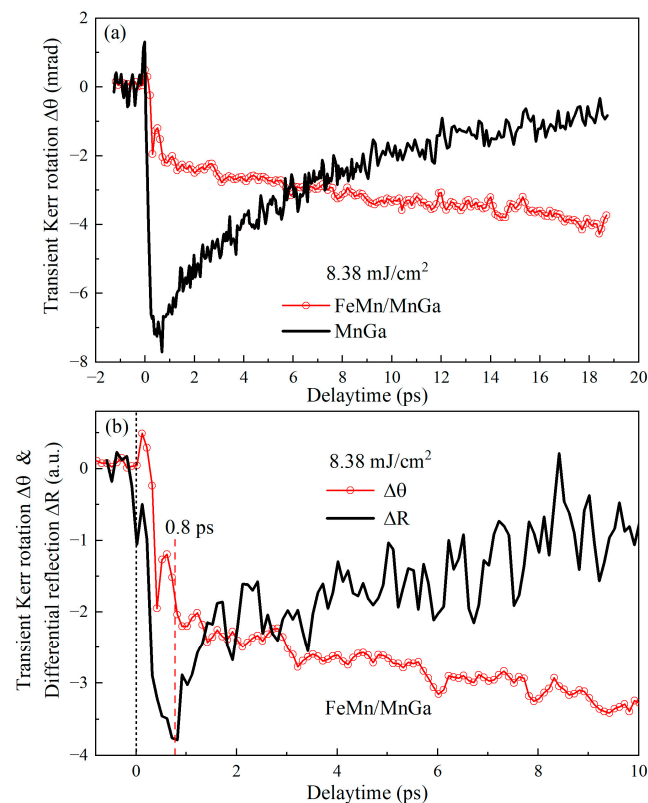


Figure 3. (a) The ultrafast demagnetization dynamics of FeMn/MnGa (open circles) and MnGa (solid line). (b) Short temporal traces of the Kerr signal (open circles) and transient reflectivity (solid line) of FeMn/MnGa upon photoexcitation.

3.1. Modeling of the Ultrafast Dynamics of Magnetization

To understand the ultrafast dynamics of demagnetization quantitatively, it is necessary to extract the time constants and amplitudes of the fast and slower demagnetization processes. A phenomenological model including two demagnetization processes has been developed, and written as:

$$S_k(t) = C(t) \otimes \left\{ \theta(t) \bullet \left\{ A_f \left[\exp\left(-\frac{t}{\tau_f}\right) - 1 \right] + A_s \left[\exp\left(-\frac{t}{\tau_s}\right) - 1 \right] \right\} \right\} \quad (1)$$

where the term in the first square bracket describes the dynamics of fast demagnetization with a time constant of τ_f , and a demagnetization amplitude of A_f , while the term in the second square bracket denotes the dynamics of slow demagnetization with a time constant of τ_s , and a demagnetization amplitude of A_s . $\theta(t)$ is a unit-step function, and $C(t)$ represents the cross-correlation function of pump and probe pulses and can be approximated by a Gaussian function. Symbol \otimes denotes the operation of the convolution.

The two-step demagnetization can be fitted well with Equation (1) using the Origin commercial software for scientific data analysis, as colored solid lines shown in Figure 2. The four extracted parameters, A_f , A_s , τ_f and τ_s as a function of pump fluence are plotted in Figure 4 by the scattered points. One can see that the time constant (τ_f) of the fast demagnetization process is about 160 fs within experimental errors, and seems independent of pump fluence, as shown in Figure 4b, supporting the assertion that the mechanism of fast demagnetization originates from intrinsic spin flips [4,7]. However, the time constant of the slower demagnetization, τ_s , occurs at a timescale of 8–16 ps, increasing with pump fluence. Such an increase in τ_s with pump fluence agrees well with electron (FeMn)–phonon (FeMn)–couplings as the origin of the slower demagnetization because the higher pump fluence can generate a higher density of phonons that cause the enhancement of the re-absorption of phonons by electrons. Such an enhancement of the re-absorption of phonons slows down the process of electron-phonon thermal equilibrating in the FeMn layer due to the reverse flow of energy. Such a slowing of the electron-phonon thermal equilibrating process certainly causes the slowing down of subsequent phonon (FeMn)–mediated spin flips in the MnGa layer.

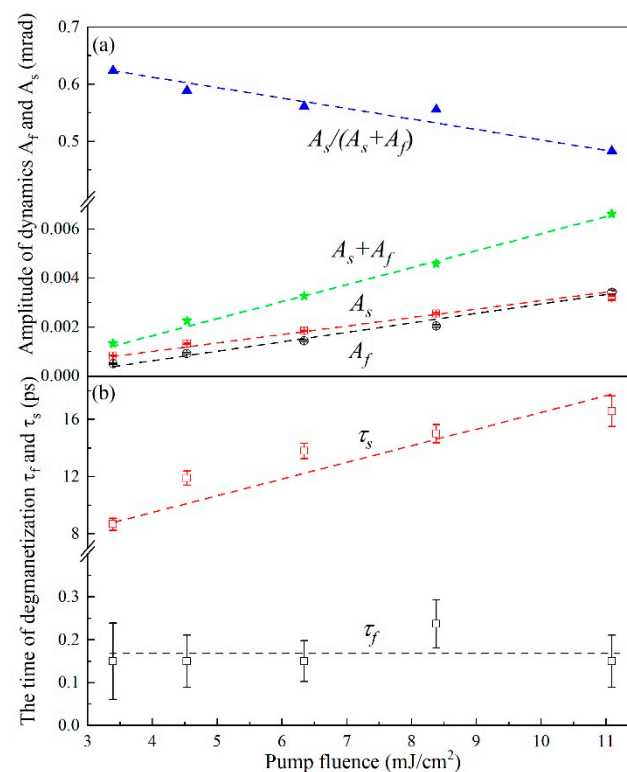


Figure 4. (a) The amplitudes of fast demagnetization (open circles, A_f) and slow demagnetization (open squares, A_s) versus the pump fluence. (b) The relaxation time τ_f and τ_s for laser-induced demagnetization are given as a function of the pump fluence. The dashed lines are the guiding eye.

One can also see that A_s is slightly stronger than A_f . A_s and A_f increase almost linearly with pump fluence. Such an increase trend should be reasonable because the strength of the first-step fast demagnetization via electron–spin coupling is related to the excited electron density, whereas the strength of the second-step demagnetization via the interlayer phonon transport should also be almost linearly dependent on the excited electron density. On the other hand, it is notable that the proportion of the slower demagnetization in the total demagnetization varies with pump fluence. The ratio, $A_s/(A_f + A_s)$, reduces from 0.624 to 0.483 with increasing pump fluence, which agrees well with the increase in τ_s . The increase in τ_s suggests more energy dissipated into environments or more energy losses which leads to the reduction in the increment of the second-step slower rise of the spin temperature.

3.2. Simulation Calculations Based on the Four-Temperature Model

To understand the microscopic mechanism of ultrafast two-step demagnetization, especially the exact energy transfer path in the second-step demagnetization, it was necessary to develop a model and to simulate the ultrafast dynamics of the two-step demagnetization quantitatively using this model. It has already been reported that the ultrafast dynamics of demagnetization in a single layer of ferromagnetic film could be well described by a 3T-M [1]. Here, an antiferromagnetic FeMn layer was added in our FeMn/MnGa bilayer film structure, and it contained two subsystems of electrons and phonons. In principle, an extended five-temperature model can describe well the ultrafast dynamics of demagnetization of our FeMn/MnGa bilayer film structure. However, the two electron subsystems, respectively, in the FeMn and MnGa layers, can be merged into one because the superdiffusive electron and spin transport between the FeMn and MnGa layers can be ignored due to the extremely short diffusion length of electrons and spins in FeMn. As a result, a four-temperature model (4T-M) is enough to describe the ultrafast dynamics of demagnetization in our bilayer structure. Based on 3T-M [1], our 4T-M can be written as:

$$\begin{aligned} C_e(T_e) \frac{dT_e}{dt} &= -G_{es}(T_e - T_s) - G_{el}(T_e - T_l) + P(t) - G_{el}^{FeMn}(T_e - T_l^{FeMn}) \\ C_l \frac{dT_l}{dt} &= -G_{el}(T_l - T_e) - G_{sl}(T_l - T_s) - G_{ll}(T_l - T_l^{FeMn}) \\ C_s \frac{dT_s}{dt} &= -G_{es}(T_s - T_e) - (T_s - T_l) - G_{sl}^{FeMn}(T_s - T_l^{FeMn}) \\ C_l^{MnFe} \frac{dT_l^{FeMn}}{dt} &= -G_{el}^{FeMn}(T_l^{FeMn} - T_e) - G_{sl}^{FeMn}(T_l^{FeMn} - T_s) - G_{ll}(T_l^{FeMn} - T_l) \end{aligned} \quad (2)$$

where C_e , C_s , C_l and C_l^{FeMn} are the specific heats of the electrons, spins, lattice (phonon) subsystems of MnGa and lattice subsystem of FeMn, respectively, while T_e , T_s , T_l and T_l^{FeMn} are their respective temperatures. G_{es} , G_{el} , G_{sl} , G_{el}^{FeMn} and G_{sl}^{FeMn} are the coupling constants of the electron–spin, electron–lattice and spin–lattice interactions in the MnGa layer, the electron–lattice in the FeMn layer and the spin–lattice interactions between FeMn and MnGa layers, respectively. G_{ll} is an effective phonon–phonon exchange coupling due to phonon transport. $P(t)$ is the pump power absorbed by the electron subsystem per unit volume.

The first three equations in Equation (2) are just the modified 3T-M in the MnGa layer with the last term added in each equation to take account for the coupling interaction with phonons in the FeMn layer, while the fourth or last equation is newly added to describe the time evolution of the temperature of the phonon subsystem and the coupling interaction of phonons in the FeMn layer with the electron, spin and phonon subsystems in the MnGa layer. In simulation calculations, $P(t)$ was approximated by the Gaussian form, $P(t) = \frac{P_0}{\sigma\sqrt{2\pi}} \exp\left(-\frac{t^2}{2\sigma^2}\right)$. $C_l = 1.83 \times 10^6 \text{ J(m}^{-3}\text{K}^{-1})$ and $C_l^{FeMn} = 1.77 \times 10^6 \text{ J(m}^{-3}\text{K}^{-1})$ were set fixed based on the Debye law [32,33], while $C_e(T_e) = \gamma T_e$ and $\gamma = 479 \text{ J(m}^{-3}\text{K}^{-2})$ were set [32,33]. The specific heat of the spins, $C_s = 2.32 \times 10^5 \text{ J(m}^{-3}\text{K}^{-1})$ in the MnGa film was calculated by $C_s = C_{tol} - C_e(T = 300 \text{ K}) - C_l$ [33,34], where C_{tol} is $\sim 2.2 \times 10^6 \text{ J(m}^{-3}\text{K}^{-1})$ [33]. The coupling constants between the electron and phonon subsystem were calculated by $G_{el} = \frac{3\pi D_F^2 D_p k_B^2 T_D \lambda_{ep}^2}{2\hbar}$ [13,22], where k_B is the Boltzmann constant, T_D is the Debye temperature ($T_D = 275 \text{ K}$ [33]; $T_D^{FeMn} = 560 \text{ K}$ [32]), D_F is the density of states at the Fermi level ($D_F = 1 \text{ eV}^{-1}\text{atom}^{-1}$ [33,35]; $D_F^{FeMn} = 2 \text{ eV}^{-1}\text{atom}^{-1}$ [36], $D_p = 3$ [22] is the number of oscillators per atomic site and λ_{ep} is the electron–phonon coupling constant ($\lambda_{ep} = 0.04 \text{ eV}$ [27,35]; $\lambda_{ep}^{FeMn} = 0.1 \text{ eV}$ [37,38]). Consequently, G_{el} and G_{el}^{FeMn} were calculated as $\sim 1.7 \times 10^{16} \text{ W(m}^{-3}\text{K}^{-1})$ and $\sim 9.4 \times 10^{17} \text{ W(m}^{-3}\text{K}^{-1})$, respectively. $G_{es} = 1.7 \times 10^{17} \text{ W(m}^{-3}\text{K}^{-1})$ was taken reasonably according to Ref. [1]. The phonon transport term or the interlayer phonon–phonon interaction, G_{ll} can be written as $G_{ll} = \frac{\xi_p}{L_p^2} (8.3 \times 10^{17} \text{ W(m}^{-3}\text{K}^{-1}))$, where $\xi_p = 30 \text{ W(m}^{-1}\text{K}^{-1})$

and $L_p = 6$ nm was taken reasonably according to Refs. [31,39] for our sample. $\sigma = 43$ fs and $P_0 = 1 \times 10^7$ mJ/cm³ were set. The remaining two parameters, G_{sl} and G_{sl}^{FeMn} were tuned until the ultrafast dynamics of two-step demagnetization were closely reproduced.

Simulation calculations were performed based on 4T-M in Equation (2) for different values of G_{sl} and G_{sl}^{FeMn} . It was found that the time evolution of T_s presented an ultrafast two-step rising process that corresponded to an ultrafast two-step demagnetization due to a linear correlation between T_s and magnetization when G_{sl} was in order of 1.0×10^{16} W(m⁻³K⁻¹) and G_{sl}^{FeMn} was in order of 1.0×10^{14} W(m⁻³K⁻¹). At this moment, by adjusting G_{sl} and G_{sl}^{FeMn} carefully, the ultrafast dynamics of two-step demagnetization were reproduced well as $G_{sl} = 1.5 \times 10^{16}$ W(m⁻³K⁻¹) and $G_{sl}^{FeMn} \leq 5.4 \times 10^{14}$ W(m⁻³K⁻¹). Simulating results are plotted in Figures 5a and 5b, respectively, for the FeMn/MnGa bilayer and single MnGa films. One can see clearly the time evolution of the temperatures of the four subsystems of electrons, spins, phonons in MnGa and phonons in FeMn from Figure 5a. The temperature of the electron subsystem, T_e , first rises sharply in 200 fs after pump excitation, as the black dashed line shows. Meanwhile, the temperature of the spin subsystem, T_s , also performs the first-step fast rising within $\Delta t_1 = \sim 600$ fs, as the red line shows in the Δt_1 window, while the temperature of the phonon subsystem in the FeMn layer, T_l^{FeMn} , also rises sharply up to a peak temperature in the Δt_1 interval via the strong electron–phonon coupling, as the green dash-dot line shows. T_l is smaller than T_s in the Δt_1 window, implying that the first-step demagnetization is possibly driven via intralayer phonons, but only possibly via electrons and interlayer phonons because of $T_e > T_s$, and $T_l^{FeMn} > T_s$. However, good simulations were obtained under the condition of $G_{sl}^{FeMn} \leq 5.4 \times 10^{14}$ W(m⁻³K⁻¹). So a small $G_{sl}^{FeMn} \leq 5.4 \times 10^{14}$ W(m⁻³K⁻¹) implies that the interlayer phonon–spin coupling channel is closed. Consequently, the first-step fast demagnetization can only come from electron–spin coupling, agreeing well with the experimental results in Figure 3. After the Δt_1 interval, T_l and T_s keep increasing slowly, but T_l increases faster than T_s and becomes obviously higher than T_s , leading to an energy transfer from phonons in the MnGa layer to spin. Therefore, this simulation revealed that the second-step slow demagnetization originates from phonon (FeMn)–phonon (MnGa)–spin coupling. To clearly show the two-step process of T_s rising, T_s is alone plotted in Figure 5b. Its fit with the single exponential and double-exponential sums in Equation (1) functions are also plotted in Figure 5b by blue dash and black dot lines, respectively. The double-exponential sum function fits the simulation data very well, but the single exponential function fails to fit well. The good double-exponential fit gives the time constants of fast and slow processes as $\tau_f = \sim 0.46$ ps and $\tau_s = \sim 8.39$ ps, respectively, while the ratio of the amplitude (A_s) of the slow component to the total increment ($A_f + A_s$), $A_s/(A_f + A_s)$ reaches ~ 0.56 . These parameters agree well with those in Figure 4 at the pump fluence of 3.39 mJ/cm².

To intuitively reveal the origin of the second-step slow demagnetization, we studied the effect of the magnitude of the phonon (FeMn)–spin coupling coefficient (G_{sl}^{FeMn}) on the second-step slow demagnetization process or the second-step slow rising process of T_s . As the blue dash line shows in Figure 5c, the second-step slow rising accelerates as G_{sl}^{FeMn} increases to 5.4×10^{16} W(m⁻³K⁻¹) which implies the phonon (FeMn)–spin (MnGa) coupling channel is opened. It disappears and the first-step fast process enhances as G_{sl}^{FeMn} increases to 5.4×10^{17} W(m⁻³K⁻¹) and above, as the magenta dot-dashed and green lines show, respectively. The enhancement of G_{sl}^{FeMn} means the weakening of energy transfer via the phonon (FeMn)–phonon (MnGa)–spin coupling channel, leading to the disappearance of the second-step slow rising process of T_s . This intuitively shows that the second-step slow demagnetization process originates from phonon transport via the phonon (FeMn)–phonon (MnGa)–spin coupling channel, rather than from phonon (FeMn)–spin coupling.

We also carried out the simulation calculations of ultrafast demagnetization dynamics in a single layer of MnGa by turning off all the coupling channels between the FeMn and MnGa layers by setting $G_{el}^{FeMn} = 0$, $G_{ll} = 0$ and $G_{sl}^{FeMn} = 0$, and maintaining all the other parameters consistent with those used in Figure 5a except for reducing P_0 to deduct the absorbed energy of the FeMn layer. The simulation results are plotted in Figure 5d. T_s

obviously presents the ultrafast dynamics of one-step demagnetization, as the red line shows, agreeing well with experimentally measured one-step ultrafast demagnetization in a single MnGa layer as shown in Figure 3a. Such a good agreement shows the validity of our 4T-M and the rationalities of all parameters used in the calculations.

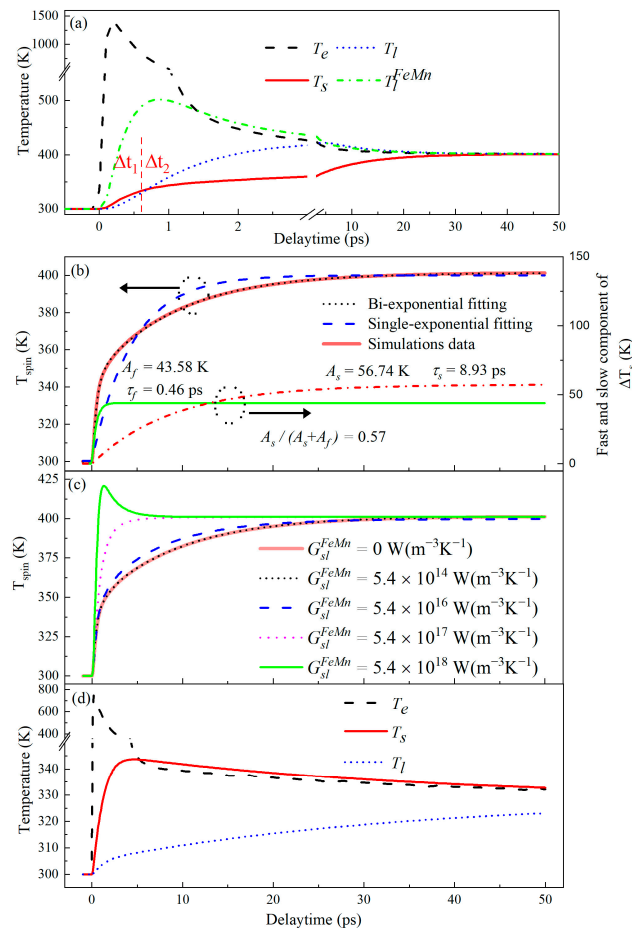


Figure 5. (a) Simulation temperature time evolution of electron (dash line), lattice of MnGa (dot line), lattice of FeMn (dot-dashed line), and spin (solid line) in an FeMn/MnGa layered structure at a pump fluence of 3.39 mJ/cm^2 in a 4T-M model. The time window is divided into two regions Δt_1 and Δt_2 for convenient discussions. (b) The temperature in the spin system alone (red solid line). The blue dash and black dot lines are fits of a single- and double-exponential sum function in Equation (1) functions, respectively. (c) Simulation time evolution of the spin temperature in an FeMn/MnGa layered structure at various phonon (FeMn)-spin coupling coefficient (G_{sl}^{FeMn}) values in a 4T-M model. (d) Simulations of the time evolution of electron (dash line), lattice (dot line) and spin (solid line) temperatures in a sole MnGa layer by 4T-M as all coupling channels between the FeMn and MnGa layers are turned off.

4. Conclusions

An antiferromagnet/ferromagnet bilayer nanostructure, FeMn/MnGa film, was designed and grown on a GaAs substrate by MBE. MBE growth guaranteed the consistency of the lattice structure in the FeMn and MnGa layers. In other words, almost no phonon scattering occurred at the magnetic interface of the FeMn/MnGa heterostructure so that phonons could transport easily from the FeMn into the MnGa layers. An FeMn antiferromagnetic layer was selected to suppress possible electron and spin transports because of the extremely short diffusion length of electrons and spins in the antiferromagnetic materials. The ultrafast dynamics of demagnetization were studied on the FeMn/MnGa bilayer and MnGa single layer films comparatively with TR-MOKE spectroscopy. The ultrafast dynamics of two-step demagnetizations, including the first-step fast and the second-step

slow demagnetizations, were observed on the FeMn/MnGa film, whereas only the ultrafast dynamics of the first-step fast demagnetization occurred on the single MnGa film. These comparative results reveal that the first-step fast demagnetization originates from the sole MnGa layer, while the second-step slow demagnetization comes from phonon transport because possible electron and spin transports are suppressed in FeMn antiferromagnetic films, and they should occur in a subpicosecond time scale. Transient reflectivity reveals that the ultrafast rising process of the temperature of excited electrons agrees well with the first-step fast demagnetization, implying that the first-step fast demagnetization originates from electron–spin coupling. To understand the exact path of FeMn-phonon-mediation of the second-step slow demagnetization, we developed a four temperature model considering phonon transport on the basis of 3T-M. Simulation calculations were performed based on this 4T-M, and reproduced well the ultrafast dynamics of two-step demagnetization observed as the phonon (FeMn)–spin (MnGa) coupling channel was closed. However, the second-step slow demagnetization accelerated until it became fast and occurred in a subpicosecond time scale as the phonon (FeMn)–spin (MnGa) coupling channel opened and its coupling strength increased. This indicates that the second-step slow demagnetization originates from FeMn phonon–phonon (MnGa)–spin coupling. In other words, we observed ultrafast demagnetization driven by phonon transport in an FeMn/MnGa bilayer structure.

Author Contributions: Conceptualization, T.L. and J.Z.; methodology, T.J. and Z.C.; software, T.J. and Z.C.; formal analysis, T.J., X.Z. and Y.Y.; investigation, T.J.; resources, X.Z.; data curation, T.L. and J.Z.; writing—original draft preparation, T.J.; writing—review and editing, T.L.; supervision, T.L. and J.Z.; project administration, T.L.; funding acquisition, T.L. All authors have read and agreed to the published version of the manuscript.

Funding: This research was funded by the National Natural Science Foundation of China (grant No. 11774438 and 12074441) as well as the Guangdong Basic and Applied Basic Foundation in China (grant No. 2019A1515011572), and was also partially supported by the National Key R&D Program of China (grant No.2018YFB0407601), and the Strategic Priority Research Program of the Chinese Academy of Sciences (Grant No. XDB44000000).

Data Availability Statement: The data presented in this study are available on request from the corresponding author.

Conflicts of Interest: The authors declare no conflict of interest.

References

1. Beaurepaire, E.; Merle, J.; Daunois, A.; Bigot, J.Y. Ultrafast spin dynamics in ferromagnetic nickel. *Phys. Rev. Lett.* **1996**, *76*, 4250–4254. [[CrossRef](#)] [[PubMed](#)]
2. Wang, Z.X.; Li, J.M.; Deng, J.Q.; Chen, Z.F.; Lai, T.S. Synchronized time- and high-field-resolved all-optical pump-probe magneto-optical setup based on a strong alternating magnetic field and its application in magnetization dynamics of high coercivity magnetic medium. *Rev. Sci. Instrum.* **2011**, *82*, 034703–034709. [[CrossRef](#)] [[PubMed](#)]
3. Guidoni, L.; Beaurepaire, E.; Bigot, J.Y. Magneto-optics in the ultrafast regime: Thermalization of spin populations in ferromagnetic films. *Phys. Rev. Lett.* **2002**, *89*, 017401–017405. [[CrossRef](#)] [[PubMed](#)]
4. Zhang, Q.; Nurmikko, A.V.; Miao, G.X.; Xiao, G.; Gupta, A. Ultrafast spin-dynamics in half-metallic CrO₂ thin films. *Phys. Rev. B* **2006**, *74*, 064414–064420. [[CrossRef](#)]
5. Radu, I.; Vahaplar, K.; Stamm, C.; Kachel, T.; Pontius, N.; Durr, H.A.; Ostler, T.A.; Barker, J.; Evans, R.F.; Chantrell, R.W.; et al. Transient ferromagnetic-like state mediating ultrafast reversal of antiferromagnetically coupled spins. *Nature* **2011**, *472*, 205–210. [[CrossRef](#)]
6. Liu, S.; Song, L.; Kong, C.T.; Zhao, X.P.; Wang, H.L.; Zhao, J.H.; Zhang, X.H. The enhanced ultrafast demagnetization at low temperature for MBE-grown Co₂FeAl film on GaAs. *Phys. B Condens. Matter* **2022**, *646*, 414308. [[CrossRef](#)]
7. Liu, X.D.; Xu, Z.; Gao, R.X.; Hu, H.N.; Chen, Z.F.; Wang, Z.X.; Du, J.; Zhou, S.M.; Lai, T.S. Dynamics of magnetization, reversal, and ultrafast demagnetization of TbFeCo amorphous films. *Appl. Phys. Lett.* **2008**, *92*, 232501–232504. [[CrossRef](#)]
8. Chen, Z.F.; Li, S.F.; Zhou, S.M.; Lai, T.S. Ultrafast dynamics of 4f electron spins in TbFeCo film driven by inter-atomic 3d-5d-4f exchange coupling. *New J. Phys.* **2019**, *21*, 123007–123016. [[CrossRef](#)]
9. Kim, J.W.; Lee, K.D.; Jeong, J.W.; Shin, S.C. Ultrafast spin demagnetization by nonthermal electrons of TbFe alloy film. *Appl. Phys. Lett.* **2009**, *94*, 192506–192509. [[CrossRef](#)]

10. Mekonnen, A.; Khorsand, A.R.; Cormier, M.; Kimel, A.V.; Kirilyuk, A.; Hrabec, A.; Ranno, L.; Tsukamoto, A.; Itoh, A.; Rasing, T. Role of the inter-sublattice exchange coupling in short-laser-pulse-induced demagnetization dynamics of GdCo and GdCoFe alloys. *Phys. Rev. B* **2013**, *87*, 180406–180411. [[CrossRef](#)]
11. Atxitia, U.; Chubykalo-Fesenko, O.; Walowski, J.; Mann, A.; Munzenberg, M. Evidence for thermal mechanisms in laser-induced femtosecond spin dynamics. *Phys. Rev. B* **2010**, *81*, 174401–174409. [[CrossRef](#)]
12. Krauß, M.; Roth, T.; Alebrand, S.; Steil, D.; Cinchetti, M.; Aeschlimann, M.; Schneider, H.C. Ultrafast demagnetization of ferromagnetic transition metals: The role of the Coulomb interaction. *Phys. Rev. B* **2009**, *80*, 180407–180411. [[CrossRef](#)]
13. Koopmans, B.; Malinowski, G.; Dalla Longa, F.; Steiauf, D.; Fahle, M.; Roth, T.; Cinchetti, M.; Aeschlimann, M. Explaining the paradoxical diversity of ultrafast laser-induced demagnetization. *Nat. Mater.* **2010**, *9*, 259–266. [[CrossRef](#)] [[PubMed](#)]
14. Battiato, M.; Carva, K.; Oppeneer, P.M. Superdiffusive spin transport as a mechanism of ultrafast demagnetization. *Phys. Rev. Lett.* **2010**, *105*, 027203–027207. [[CrossRef](#)]
15. Shokeen, V.; Sanchez Piaia, M.; Bigot, J.Y.; Muller, T.; Elliott, P.; Dewhurst, J.K.; Sharma, S.; Gross, E.K.U. Spin Flips versus Spin Transport in Nonthermal Electrons Excited by Ultrashort Optical Pulses in Transition Metals. *Phys. Rev. Lett.* **2017**, *119*, 107203–107208. [[CrossRef](#)] [[PubMed](#)]
16. Melnikov, A.; Razdolski, I.; Wehling, T.O.; Papaioannou, E.T.; Roddatis, V.; Fumagalli, P.; Aktsipetrov, O.; Lichtenstein, A.I.; Bovensiepen, U. Ultrafast transport of laser-excited spin-polarized carriers in Au/Fe/MgO(001). *Phys. Rev. Lett.* **2011**, *107*, 076601–076606. [[CrossRef](#)]
17. Jiang, T.R.; Zhao, X.P.; Chen, Z.F.; You, Y.Y.; Lai, T.S.; Zhao, J.H. Ultrafast enhancement and optical control of magnetization in ferromagnet/semiconductor layered structures via superdiffusive spin transports. *Mater. Today Phys.* **2022**, *26*, 100723. [[CrossRef](#)]
18. Melnikov, A.; Brandt, L.; Liebing, N.; Ribow, M.; Mertig, I.; Woltersdorf, G. Ultrafast spin transport and control of spin current pulse shape in metallic multilayers. *Phys. Rev. B* **2022**, *106*, 104417. [[CrossRef](#)]
19. Turgut, E.; La-o-Vorakiat, C.; Shaw, J.M.; Grychtol, P.; Nembach, H.T.; Rudolf, D.; Adam, R.; Aeschlimann, M.; Schneider, C.M.; Silva, T.J.; et al. Controlling the competition between optically induced ultrafast spin-flip scattering and spin transport in magnetic multilayers. *Phys. Rev. Lett.* **2013**, *110*, 197201–197207. [[CrossRef](#)]
20. Rudolf, D.; La, O.V.C.; Battiato, M.; Adam, R.; Shaw, J.M.; Turgut, E.; Maldonado, P.; Mathias, S.; Grychtol, P.; Nembach, H.T.; et al. Ultrafast magnetization enhancement in metallic multilayers driven by superdiffusive spin current. *Nat. Commun.* **2012**, *3*, 1037–1043. [[CrossRef](#)]
21. Eschenlohr, A.; Battiato, M.; Maldonado, P.; Pontius, N.; Kachel, T.; Holldack, K.; Mitzner, R.; Fohlich, A.; Oppeneer, P.M.; Stamm, C. Ultrafast spin transport as key to femtosecond demagnetization. *Nat. Mater.* **2013**, *12*, 332–337. [[CrossRef](#)]
22. Bergeard, N.; Hehn, M.; Mangin, S.; Lengaigne, G.; Moutaigne, F.; Lalieu, M.L.; Koopmans, B.; Malinowski, G. Hot-Electron-Induced Ultrafast Demagnetization in Co/Pt Multilayers. *Phys. Rev. Lett.* **2016**, *117*, 147203–147208. [[CrossRef](#)] [[PubMed](#)]
23. Baltz, V.; Manchon, A.; Tsoi, M.; Moriyama, T.; Ono, T.; Tserkovnyak, Y. Antiferromagnetic spintronics. *Rev. Mod. Phys.* **2018**, *90*, 015005–015062. [[CrossRef](#)]
24. Zhang, W.; Jungfleisch, M.B.; Jiang, W.; Pearson, J.E.; Hoffmann, A.; Freimuth, F.; Mokrousov, Y. Spin Hall effects in metallic antiferromagnets. *Phys. Rev. Lett.* **2014**, *113*, 196602–196608. [[CrossRef](#)]
25. Saglam, H.; Zhang, W.; Jungfleisch, M.B.; Sklenar, J.; Pearson, J.E.; Ketterson, J.B.; Hoffmann, A. Spin transport through the metallic antiferromagnet FeMn. *Phys. Rev. B* **2016**, *94*, 140412–140417. [[CrossRef](#)]
26. Zhao, X.P.; Lu, J.; Mao, S.W.; Yu, Z.F.; Wei, D.H.; Zhao, J.H. Spontaneous perpendicular exchange bias effect in L10-MnGa/FeMn bilayers grown by molecular-beam epitaxy. *Appl. Phys. Lett.* **2018**, *112*, 042403–042408. [[CrossRef](#)]
27. Zhu, L.J.; Brandt, L.; Zhao, J.H.; Woltersdorf, G. Composition-tuned magneto-optical Kerr effect in L10-MnxGa films with giant perpendicular anisotropy. *J. Phys. D Appl. Phys.* **2016**, *49*, 245001–245006. [[CrossRef](#)]
28. Muller, G.M.; Walowski, J.; Djordjevic, M.; Miao, G.X.; Gupta, A.; Ramos, A.V.; Gehrke, K.; Moshnyaga, V.; Samwer, K.; Schmalhorst, J.; et al. Spin polarization in half-metals probed by femtosecond spin excitation. *Nat. Mater.* **2009**, *8*, 56–62. [[CrossRef](#)] [[PubMed](#)]
29. Bonfiglio, G.; Rode, K.; Atcheson, G.Y.P.; Stamenov, P.; Coey, J.M.D.; Kimel, A.V.; Rasing, T.; Kirilyuk, A. Sub-picosecond exchange-relaxation in the compensated ferrimagnet Mn₂Ru_xGa. *arXiv* **2021**, arXiv:2003.01420. [[CrossRef](#)]
30. Beyazit, Y.; Beckord, J.; Zhou, P.; Meyburg, J.P.; Kuhne, F.; Diesing, D.; Ligges, M.; Bovensiepen, U. Local and Nonlocal Electron Dynamics of Au/Fe/MgO(001) Heterostructures Analyzed by Time-Resolved Two-Photon Photoemission Spectroscopy. *Phys. Rev. Lett.* **2020**, *125*, 076803–076809. [[CrossRef](#)] [[PubMed](#)]
31. Choi, G.M.; Wilson, R.B.; Cahill, D.G. Indirect heating of Pt by short-pulse laser irradiation of Au in a nanoscale Pt/Au bilayer. *Phys. Rev. B* **2014**, *89*, 064307–064314. [[CrossRef](#)]
32. Shi, S.; Liu, C.; Wan, J.F.; Rong, Y.H.; Zhang, J.H. Thermodynamics of fcc–fcc martensitic transformation in Mn–X (X = Cu, Fe) alloys. *Mater. Des.* **2016**, *92*, 960–970. [[CrossRef](#)]
33. Winterlik, J.; Balke, B.; Fecher, G.H.; Felser, C.; Alves, M.C.M.; Bernardi, F.; Morais, J. Structural, electronic, and magnetic properties of tetragonal Mn_{3–x}Ga: Experiments and first-principles calculations. *Phys. Rev. B* **2008**, *77*, 054406–054418. [[CrossRef](#)]
34. Seixas, T.M.; da Silva, M.A.S.; de Lima, O.F.; Lopez, J.; Braun, H.F.; Eska, G. Specific heat of Gd₄Co₃. *J. Phys. D: Appl. Phys.* **2010**, *22*, 136002–136009. [[CrossRef](#)]

35. Mizukami, S.; Wu, F.; Sakuma, A.; Walowski, J.; Watanabe, D.; Kubota, T.; Zhang, X.; Naganuma, H.; Oogane, M.; Ando, Y.; et al. Long-lived ultrafast spin precession in manganese alloys films with a large perpendicular magnetic anisotropy. *Phys. Rev. Lett.* **2011**, *106*, 117201–117205. [[CrossRef](#)]
36. Malonda-Boungou, B.R.; Binggeli, N.; M'Passi-Mabiala, B. Noncollinear magnetic structures of FeMn ultrathin films on Cu(001). *Superlattices Microstruct.* **2016**, *100*, 767–779. [[CrossRef](#)]
37. Ritzmann, U.; Oppeneer, P.M.; Maldonado, P. Theory of out-of-equilibrium electron and phonon dynamics in metals after femtosecond laser excitation. *Phys. Rev. B* **2020**, *102*, 214305–214319. [[CrossRef](#)]
38. Medvedev, N.; Milov, I. Electron-phonon coupling in metals at high electronic temperatures. *Phys. Rev. B* **2020**, *102*, 214305–214327. [[CrossRef](#)]
39. Wu, B.M.; Yang, D.S.; Sheng, S.; Du, Y.L.; Xu, W.M. The transport properties and internal friction related to the antiferromagnetic transition in $\text{Cr}_{75}(\text{Fe}_x\text{Mn}_{1-x})_{25}$ alloys. *J. Magn. Magn. Mater.* **1999**, *202*, 426–430. [[CrossRef](#)]